2170
doi:10.1017/S1431927621007819
Microsc. Microanal. 27 (Suppl 1), 2021

Direct observation of the perpendicular shape anisotropy and thermal stability of STT-MRAM nano-pillars examined by off-axis electron holography

Trevor Almeida[1], Steven Lequeux[2], Alvaro Palomino[2], Nuno Caçoilo[2], Aurélien Massebouef[2], Richard Sousa[2], Olivier Fruchart[2], Ioan-Lucian Prejbeanu[2], Bernard Dieny[3] and David Cooper[4]

[1]Univ. Grenoble Alpes, CEA, Leti, F-38000 Grenoble, France., France, [2]Univ Grenoble Alpes, CEA, CNRS, Grenoble INP, SPINTEC, 38000 Grenoble, France., France, [3]Univ Grenoble Alpes, CEA, CNRS, Grenoble INP, SPINTEC, 38000 Grenoble, France., Grenoble, France, [4]Univ Grenoble Alpes, CEA, LETI, France

Magnetic random-access memory (MRAM) is a non-volatile memory based on the storage of one bit of information by a ferromagnetic memory carrier. In particular, spin-transfer torque (STT) MRAM has attracted great interest by the microelectronics industry as a replacement for embedded FLASH memory. Out-of-plane STT-MRAM involves the use of a magnetic tunnel junction (MTJ) comprising an MgO tunnel barrier (1 – 1.5 nm) sandwiched between two thin perpendicularly-magnetized layers: one magnetically-pinned reference layer, and one switchable storage layer. The electrical resistance of the MTJ changes significantly when the layers are magnetized in parallel and antiparallel states, providing a system of readable / writable '0' or '1' binary information. The areal bit density of modern STT-MRAM can be improved further by reducing the in-plane size of the MTJ, which however may reduce the thermal stability of the storage layer. One solution is to increase the storage layer thickness to larger than its diameter so that its out-of-plane aspect ratio provides additional thermal stability through perpendicular shape anisotropy (PSA). Previous studies have shown that the PSA-STT-MRAM are indeed highly thermally stable, making them an exciting solution to downsize scalability of STT-MRAM at sub-20 nm technology nodes[1,2]. However, our knowledge of the thermal stability of these STT-MRAM nano-pillars is often indirect, relying on magnetoresistance measurements and micromagnetic modelling. In order to understand fully their thermomagnetic behavior, it is necessary to examine the effect of temperature directly. The advanced transmission electron microscopy (TEM) technique of off-axis electron holography allows imaging of magnetization within nano-scale materials. Here, we use electron holography to image the micromagnetic configuration of the nano-pillars in presence of PSA and to visualize its thermal stability through *in-situ* heating.

A series of nano-pillar arrays were investigated: 1) etched Co / FeCoB / Co stacks; 2) Co nano-pillars grown within pores of a structured substrate surface; and 3) etched FeCoB / NiFe stacks. TEM samples were prepared by depositing a protective layer (~ 1 µm) of resin on the array prior to a protective Pt layer being deposited by the focused ion beam (FIB). Cross-sectional TEM lamellae were transferred to Omniprobe copper slots and thinned to < 100 nm (sample 2) or ~ 300 nm (samples 1 & 3) using conventional FIB methods. The protective resin layer was removed by plasma etching and the remaining Pt layer was broken with the micromanipulator. Scanning TEM (STEM) imaging was performed using a probe-C_S-corrected Thermo Fisher Titan TEM at 200kV, whilst energy dispersive X-ray (EDX) spectroscopy provided chemical analysis. Off-axis electron holograms were acquired under field-free conditions in Lorentz mode on a Gatan OneView 4K camera using a Thermo Fisher Titan TEM equipped with an image-C_S corrector and an electron biprism. The magnetization states of the nano-pillars were visualized through separation of the magnetic contribution to the phase shift from the mean inner potential (MIP), achieved by tilting and applying the strong field of the objective lens (< 1.5T) to reverse their magnetism. *In-situ* heating up to 250°C was performed using a Gatan heating holder under field-free magnetic conditions. The heating was repeated and the magnetic reversal was performed at each temperature interval to isolate the MIP, and subtracted from the first heating to reconstruct the thermomagnetic behavior of the nano-pillars[3,4].

Figure 1 presents magnetic induction maps reconstructed from electron holograms acquired from samples 1 & 2. The magnetic induction map of sample 1 (Fig. 1a) reveals the magnetic contours flowing through the multi-

layered Co (20 nm) / FeCoB (20 nm) / Co (25 nm) nano-pillar in a direction parallel to its long axis (indicated by white arrows), confirming its out-of-plane PSA. Fig. 1b-c presents magnetic induction maps of arrays of Co nano-pillars (~ 20 nm diameter, ~ 40 nm height) grown in pores of the substrate (sample 2). During the magnetic reversal process in Fig. 1b, a large component of the field is applied in a direction parallel to the elongated axis of the nano-pillars (red arrow). Hence, the magnetization is observed to favor this axis with adjacent nano-pillars being magnetized in parallel and antiparallel directions, perpendicular to the plane of the surface. In Fig. 1c, a large component of the field is applied parallel to the plane of the surface (red arrow) and whilst some nano-pillars retain their magnetization along their major axis, it is clear that a few nano-pillars relax into more transverse or perpendicular directions, generally flowing from left to right. In both cases, the stray fields reveal interactions between the nano-pillars and are suggested to restrict their magnetic states from relaxing along their elongated axis and in the same direction.

Figure 2 presents the morphology, chemical composition and thermal stability of an individual nano-pillar from sample 3. The schematic of Fig. 2a displays the full stack of the MTJ cell, where the thick NiFe section is deposited on a conventional stack to provide the PSA in the storage layer[2]. The STEM image (Fig. 2b) and EDX map (Fig. 2c) reveal that the NiFe section of nano-pillar is 60 nm high with a diameter of ~ 20 nm, and is separated from the hard Ta mask by a Ru layer. The magnetic induction map of Fig. 2d shows that the magnetization lies along the elongated axis of the NiFe section at 20°C, as indicated by the white arrows. Magnetic induction maps acquired during *in-situ* heating to 175°C (Fig. 2d) and 225°C (Fig. 2e) shows the nano-pillar to retain this direction of magnetization at elevated temperatures. This confirms that the high-aspect-ratio NiFe nano-pillar provides out-of-plane PSA that is thermally stable up to 225°C, and hence resistant to thermal variations during operation.

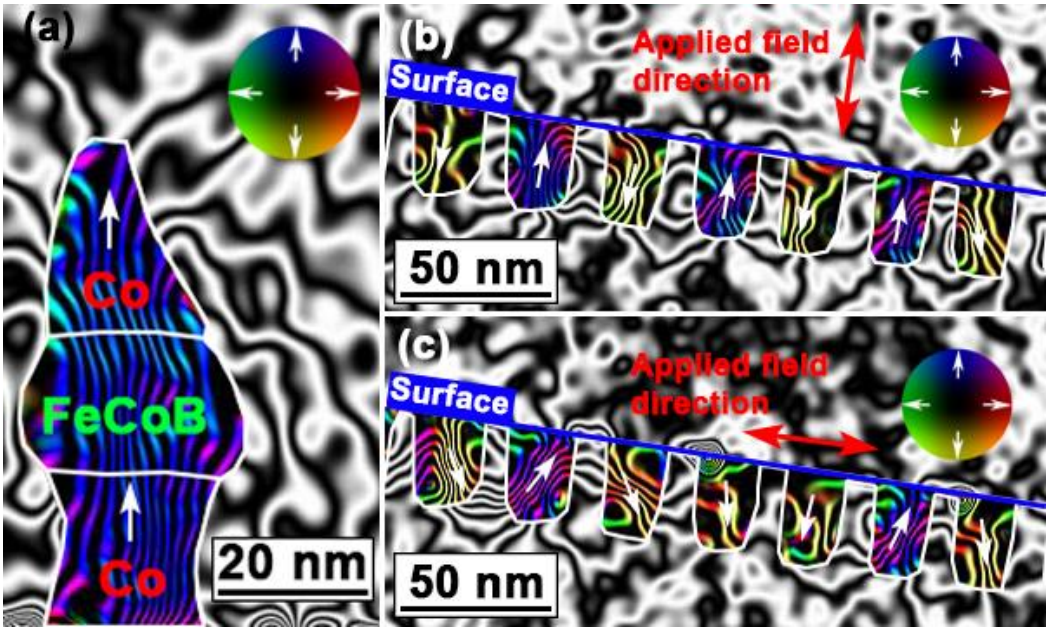

Figure 1. (a) Magnetic induction map of the multi-layered Co / FeCoB / Co nano-pillar (sample 1) showing the magnetization flowing along its elongated (i.e. vertical) axis. (b,c) Magnetic induction maps of the Co nano-pillars grown in pores of the substrate (sample 2), with a large component of the field applied in directions (b) perpendicular; and (c) parallel to the substrate surface during the magnetic reversal process (denoted by red arrows). The contour spacing is 0.042 rad for all the magnetic induction maps, and the magnetization direction is shown using white arrows, as depicted in the color wheels.

https://doi.org/10.1017/S1431927621007819 Published online by Cambridge University Press

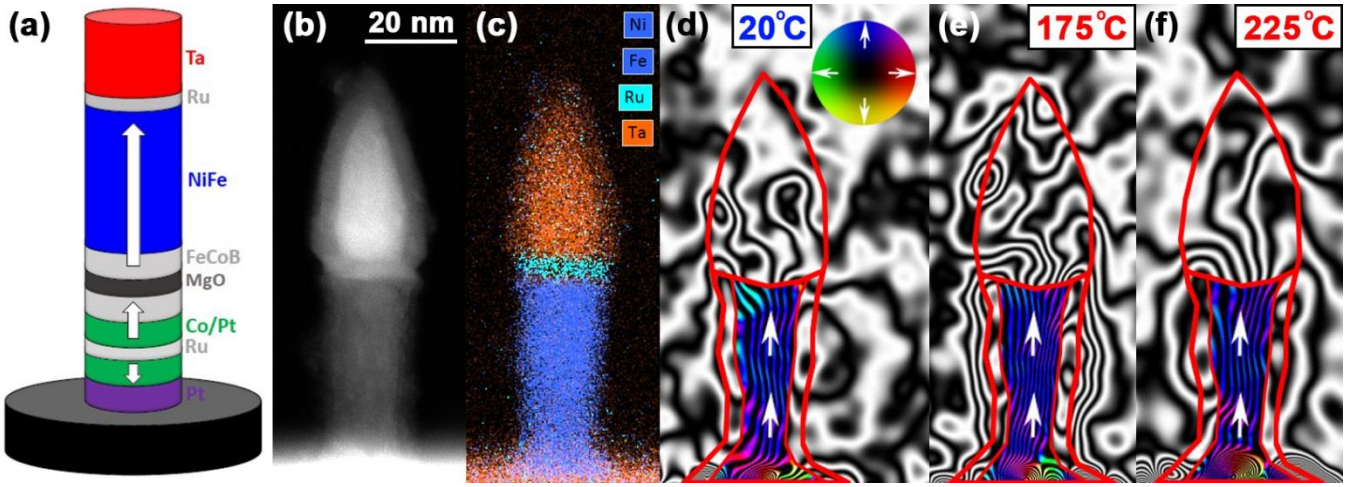

Figure 2. (a) Schematic of a PSA-STT-MRAM MTJ cell with a 60 nm NiFe storage layer, where the white arrows denote the expected magnetic easy axis2. (b) STEM image of a first PSA pillar with a diameter of ~ 20nm; and (c) the associated EDX chemical map showing the elemental distribution of Ta (red), Ni/Fe (blue) and Ru (turquoise). (d-f) Magnetic induction maps reconstructed from electron holograms acquired during in-situ heating at (d) 20°C; (e) 175°C; and (f) 225°C. The contour spacing is 0.042 rad for all the magnetic induction maps, and the magnetization direction is shown using white arrows, as depicted in the color wheel.

References

[1] N. Perrissin et al., *Nanoscale* **10**, 12187-12195 (2018).
[2] S. Lequeux et al., *Nanoscale* **12**, 6378-6384, (2020).
[3] T. P. Almeida et al., *Geophys. Res. Lett.* **43**, 8426–8434 (2016).
[4] T. P. Almeida et al., *Sci. Adv.*, **2 (4)**, e1501801 (2016).

https://doi.org/10.1017/S1431927621007819 Published online by Cambridge University Press